Materials Chemistry and Physics 120 (2010) 36–41

Contents lists available at ScienceDirect

Materials Chemistry and Physics

journal homepage: www.elsevier.com/locate/matchemphys

Preparation of self-organized porous tungsten oxide using HFCVD technique

Fernando Chávez[a], Carlos Felipe[a,b,*], Enrique Lima[c], Víctor Lara[d], Carlos Ángeles-Chávez[e], Miguel A. Hernandez[f]

[a] Departamento de Fisicoquímica de Materiales, ICUAP, Benemérita Universidad Autónoma de Puebla, Puebla, 72000, Mexico
[b] Departamento de Biociencias e Ingeniería, CIIEMAD, Instituto Politécnico Nacional, México D.F., 07340, Mexico
[c] Instituto de Investigaciones en Materiales, Universidad Nacional Autónoma de México, Circuito Exterior, Ciudad Universitaria, México D.F., 04510, Mexico
[d] Departamento de Química, Universidad Autónoma Metropolitana, Iztapalapa, México D.F., 09340, Mexico
[e] Programa de Ingeniería Molecular, Instituto Mexicano del Petroleo, México D.F., 07730, Mexico
[f] Departamento de Investigación en Zeolitas, ICUAP, Benemérita Universidad Autónoma de Puebla, Puebla, 72000, Mexico

ARTICLE INFO

Article history:
Received 16 February 2009
Received in revised form 9 October 2009
Accepted 17 October 2009

Keywords:
Tungsten oxide
Chemical vapour deposition
Porous media
Fractal dimension

ABSTRACT

Hot filament chemical vapour deposition (HFCVD) technique was applied to deposit a porous tungsten oxide film on glass wafers. The tungsten filament was used as a source in a vacuum atmosphere. The porous film was characterized by scanning electron microscopy, energy-dispersive X-ray spectroscopy, X-ray thermodiffraction, nitrogen sorption and small-angle X-ray scattering. From these characterization techniques it was found that porous film presents a clusters-like morphology of WO_{3-x} particles. The particles are arranged on substrate in a way that free spaces are originated, as a 3D network of pores. By increasing temperature, the BET specific surface area of the porous film changes from 38.67 to 34.5 $m^2\ g^{-1}$ most likely due to the particles have a tendency to stick together to form aggregates, particularly at high temperature. A fractal geometry approach permits to elucidate the interconnection between the particles and a simple model of the porous structure is proposed.

1. Introduction

The nanostructured tungsten oxide belongs to a family of semiconductors [1], which has been synthesized by different physical [2–4] and chemical [5,6] techniques. Basically, tungsten oxides exist with different morphologies such as nanowires [7,8], nanorods [9], microducts [10], and nanotubes [11]. Tungsten oxide has its unique properties such as electrical, thermal, mechanical and optical properties that are frequently used in gas-sensing applications [12,13] and electrochromic devices. Recently, many studies have been reported for this material but, an almost unexplored subject is the array or packing of primary particles leading to a porous medium which is useful to guide capillary processes such wetting and non-wetting fluids invasion [14,15]. At the same time porous tungsten enriched media are claimed in applications of heterogeneous catalysis, e.g. hydrodesulfurization of fuels [16–18], isomerization reactions [19] and photocatalytic activity [20,21]. Efforts have been made to synthesize porous tungsten oxide (PTO) in order to take advantage of its textural properties. In this way Di Fonzo et al. [22] using pulsed laser deposition (PLD), prepared nanostructured tungsten and tungsten oxide films along with the variation of pressure with different gases (Ar, He, and dry air). Berger et al. [23] reported preparation of WO_3 self-organized porous structures throughout an anodic oxidation. Authors pointed out that the semiconductor properties as well as the surface areas of their porous nanostructures have a higher efficiency to the photocurrent when applied in a photon to electron device. Pal and Jacob [24,25] prepared WO_3 nanoparticles poorly dispersed on Si and glass substrates while Deepa et al. [26] used a wet chemical route followed by an electrodeposition process to generate a WO_3 porous film. Furthermore, they reported that the porous film improves properties like the electrochromic efficiency and amplification of the optical response. Of course, a WO_3 porous film could also be promising to catalytic applications as often porous medium is the way to enhance dispersion of active sites. Then, this work was started with the goal of preparing a WO_3 porous film on a glassy substrate by packing WO_3 particles. We have applied the HFCVD technique [8,27,28] to produce PTO. The solid prepared material was characterized by scanning electron microscopy (SEM), energy-dispersive X-ray spectroscopy (EDS), X-ray thermodiffraction (XRD), nitrogen sorption and small-angle X-ray scattering (SAXS).

* Corresponding author at: Instituto Politécnico Nacional, CIIEMAD, Calle 30 de Junio de 1520 s/n Col. Barrio la Laguna Ticoman, México D.F., 07340, Mexico. Tel.: +52 55 57296000x52727; fax: +52 55 57296000x52700.
E-mail address: cfelipe98@gmail.com (C. Felipe).

0254-0584/$ – see front matter © 2009 Elsevier B.V. All rights reserved.
doi:10.1016/j.matchemphys.2009.10.017

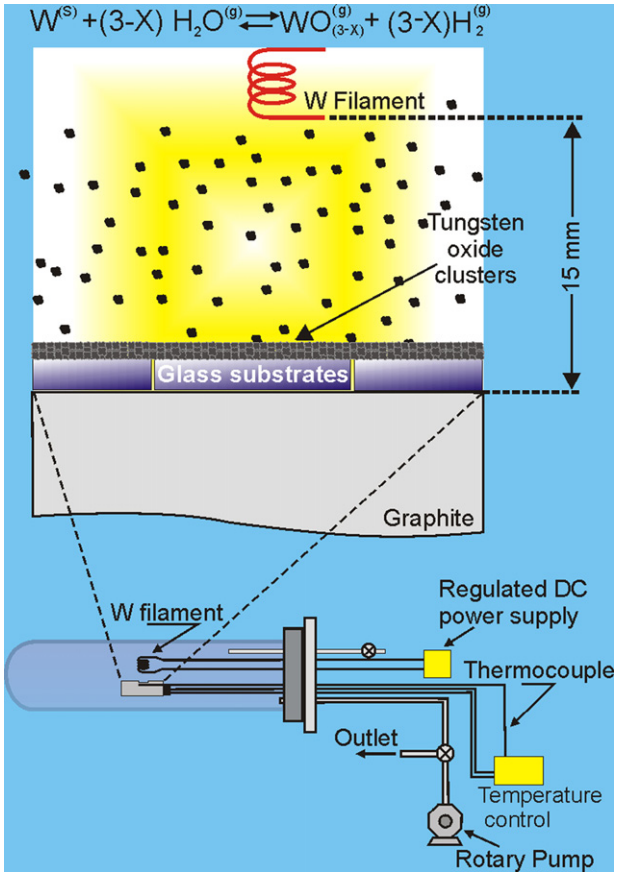

Fig. 1. Schematic diagram of the HFCVD system used for PTO film growth.

2. Experimental

2.1. Preparation of film PTO

A HFCVD system (Fig. 1) was used to prepare a PTO film with the use of a tungsten filament and a vacuum system (*ca.* 10^{-4} Torr). The W filament itself acted as a precursor for tungsten oxide and it was placed at 15 mm far from rectangular (24 mm × 40 mm × 0.15 mm) glass plates that were previously cleaned with xylene, acetone and propanol. Subsequently, a voltage (6.2 V) and a current (3.0 A) were supplied to the filament for 15 min by a regulated DC power. In this period of time the filament had a temperature close to 1000 °C (indirectly estimated with a resistivity-temperature graph-based method) and the temperature of glass substrates increased up to near 120 °C (measured with a thermocouple) as a consequence of thermal radiation. An opaque blue film was deposited on glass wafers because of the constant oxidation–sublimation process of the hot filament.

2.2. Characterization of film PTO

2.2.1. Scanning electron microscopy

SEM and EDS analyses were carried out with an environmental scanning electro-microscope (SEM, Philips XL30) equipped with an X-ray energy dispersive spectrometer (EDS).

2.2.2. X-ray diffraction

XRD patterns were recorded on a Bruker AXS D8 advance diffractometer coupled to a copper anode X-ray tube. X-ray diffraction patterns were acquired at different temperatures from 25 to 800 °C (thermodiffraction) with a temperature-scanning step of 50 °C.

2.2.3. Small angle X-ray scattering

SAXS experiments were performed using a Kratky camera coupled to a copper anode X-ray tube whose Kα radiation was selected with a nickel filter. The SAXS intensity data, $I(h)$, were collected with a linear proportional counter. Then, they were processed with the ITP program [29–33] where the scattering vector, h, is defined as $h = 4\pi \sin\theta/\lambda$, where θ and λ are the scattering angle and the X-ray wavelength, respectively. The powdered sample was introduced into a capillary tube. Measurement time was 9 min in order to obtain good quality statistics; indeed linear proportional counter is like a multichannel system therefore each point of the curve was measured for 9 min.

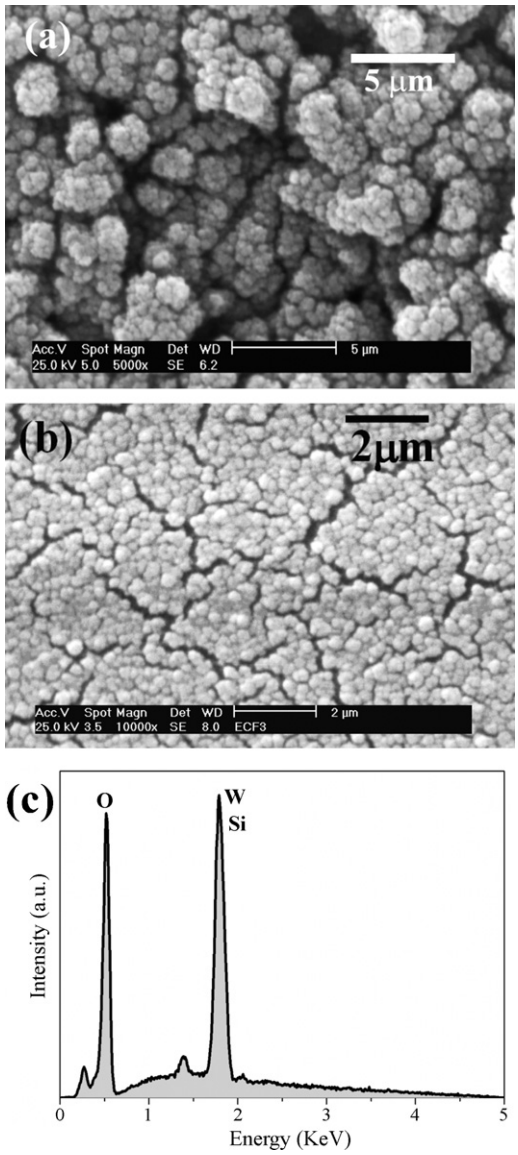

Fig. 2. SEM micrographs of PTO deposited by the HFCVD technique. (a) Low magnification, (b) high magnification and (c) EDS spectrum of PTO as deposited.

2.2.4. N_2 sorption

Ultra-high purity nitrogen gas (99.99%; Praxair) was selected to perform the sorption experiments on PTO material. To introduce the PTO sample in the appropriate N_2 adsorption cell, the original glass plates were cut into several small pieces. Prior to every sorption experiment the same sample was calcined in atmospheric air at 120, 200, 300 and 400 °C during 8 h (a heating ramp of 1 °C min^{-1} was chosen) also the PTO sample was degassed at 100 °C for 8 h previously to the adsorption run. N_2 adsorption–desorption isotherms were measured at 76 K (boiling point of nitrogen at Puebla City's 2200 m altitude) in an automatic volumetric adsorption instrument (Autosorb1-LC, Quantachrome Instruments). N_2 sorption measurements were determined in the interval of relative pressure, p/p^0, extending from 10^{-6} to 0.995. The saturation pressure, p^0, was continuously registered in the course of the adsorption–desorption measurements.

3. Results

3.1. SEM and EDS

The SEM micrographs depicted in Fig. 2 are taken immediately after depositing the PTO film on the glass plates. One can see that

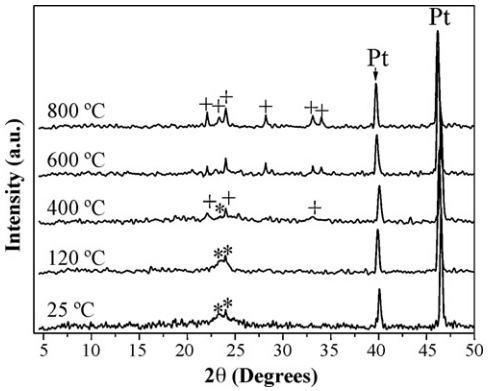

Fig. 3. XRD patterns of the PTO film calcined at different temperatures. * indicates $W_{25}O_{73}$ and + indicates WO_3, JCPDS files 71-0070 and 20-1323, respectively. Peaks labeled as platinum (Pt) are due to the holder where the sample was collocated.

the PTO is composed of particles nearly-spheroid arranged in an aggregates fashion. Nanospheres are agglomerated, apparently in a random way, originating free spaces of different sizes between the particles, as a 3D network of pores. Images at different scales permit to identify the aggregates that are formed by smaller spheres. No higher resolution images were taken than those exhibited in Fig. 2. Concerning the chemical composition of the PTO sample, EDS analysis (Fig. 2c) reveals qualitatively that the constituent elements are both oxygen and tungsten, and silicon peak comes from the substrate. A W/O ratio cannot be precisely estimated due to overlapping of tungsten and silicon peaks.

3.2. XRD pattern as a function of the temperature (thermodiffraction)

The XRD patterns of the PTO sample are shown in Fig. 3, recorded at different temperatures. At room temperature (25 °C) as well as at 120 °C, the sample is poorly crystalline but the $W_{25}O_{73}$ phase intensities are becoming more obvious to WO_3 with an increase in temperature in the range of 600–800 °C. Thus, temperature promotes a better crystallization and the oxide deficient in oxygen ($W_{25}O_{73}$) evolutes to WO_3.

3.3. SAXS experiments of sample PTO

The PTO sample was characterized by SAXS. It was treated at three different temperatures (120, 400 and 800 °C) to match the structural changes evidenced by thermodiffraction and its corresponding textural evolution. The Kratky plots of the sample are shown in Fig. 4. The scattering curve follows the Porod law, where $I(h)$ is proportional to scattering vector as a function of h^{-4} which has large h values and h^{-2} for moderate h values. Hence, the Kratky plot exhibits a clear peak in the case of scattered heterogeneities that have a globular or spheroid shape [34]. This result also agrees with the spheroid particles observed by SEM. However, it should be emphasized that, by the Babinet principle, the scattered heterogeneities could be a dense phase in a low-dense phase (particles) or a low-dense phase in a high-dense phase (bubbles, pores). Hence, we will conclude, in Section 4, that in our experiments the scattered heterogeneities correspond to the tungsten oxide particles.

On the other hand, Fig. 5 displays the size distribution of spheres as determined by SAXS, which indicated that the size of spheres is ranged mainly in diameters as small as 20–30 Å for the sample after treatment at low temperature (120 °C). When the sample was treated at higher temperature the size distribution was significantly modified, indeed

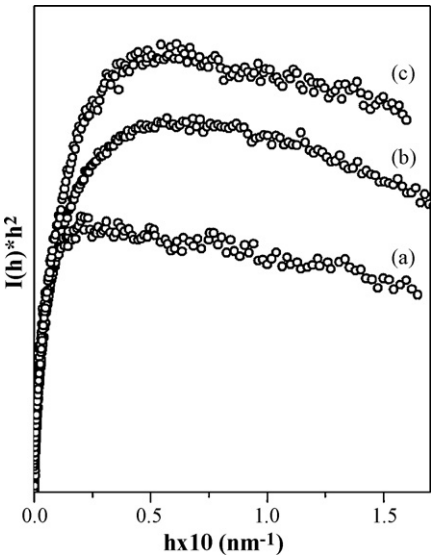

Fig. 4. Kratky plots of the same PTO sample annealing at (a) 120, (b) 400 and (c) 800 °C.

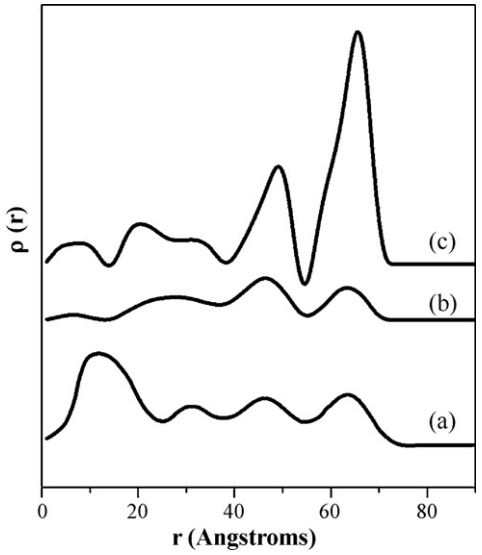

Fig. 5. Particle-size distributions, as determined from SAXS data, of the same PTO sample annealing at (a) 120, (b) 400 and (c) 800 °C.

the amount of big spheres increased in decrement of the small ones. Even though the peaks are broad, indicating a heterogeneous distribution, radius maximums at 9, 27, 48 and 66 Å.

From SAXS data, i.e. from the slope of the $\log I(h)$ *versus* $\log(h)$ curve and under the Porod law the fractal dimension [35,36] values of the scattering objects were calculated in Table 1. Fractal dimension should be understood in this work as the connectivity of the spheres. It is noticed that the fractal dimension increased with temperature.

Table 1
Fractal dimension of the same PTO sample, after thermal treatment.

Outgassing temperature (°C)	Fractal dimension
120	2.41
200	2.54
400	2.88

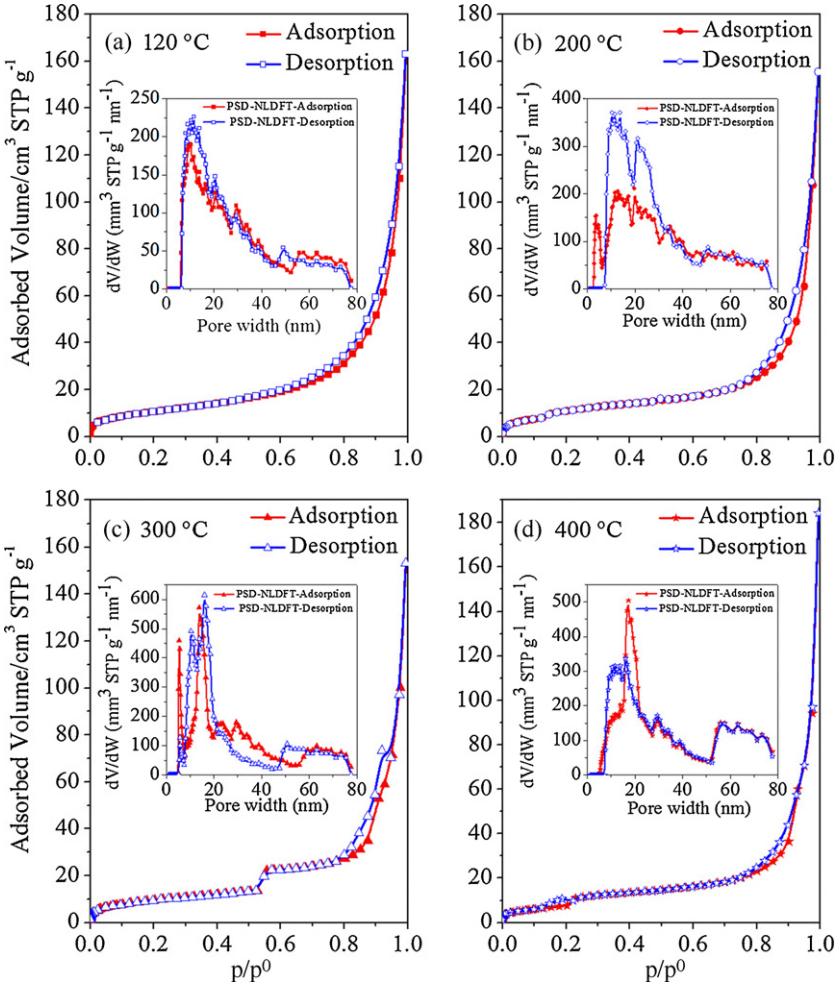

Fig. 6. N_2 sorption isotherms on same PTO film annealing at (a) 120, (b) 200, (c) 300 and (d) 400 °C. The insets show the pore size distribution (PSD) of the PTO sample. *V* represents the adsorbed volume and *W* is the pore width.

3.4. N_2 sorption characterization of sample PTO

Fig. 6 displays the N_2 adsorption–desorption isotherms carried out at 76 K and the corresponding pore size distribution as shown in Fig. 6 (inset). These sorption processes are a consequence of the field force at the surface of the porous film (adsorbent), which attracts (adsorption) or repels (desorption) the molecules of the nitrogen (adsorbate) [15,37]. The adsorptive power of the PTO depends on the area of exposed surface. Prior to the adsorption, the PTO was annealing in air at different temperatures (120, 200, 300 and 400 °C) and subjected to a degassing process. The adsorption–desorption isotherms of the same sample calcined at 120 and 200 °C corresponded to a type II in the IUPAC classification [38] having hysteresis loops type H3 which is the characteristic of capillary condensation in slit-like pores. Isotherm for sample calcined at 300 °C corresponded to type VI. The values for textural properties and pore network structural parameters of the PTO are reported in Table 2.

The nonlocal density functional theory (NLDFT) [39] has been used to determinate the pore size distribution (PSD) of the PTO sample (insets of Fig. 6a–d). This theory is based on the adsorption and phase behavior of fluids under equilibrium conditions. It should be noted that pores are sized in the range of macroporous, as well as mesoporous for the sample under study. The PSD was determined by the annealing temperature.

4. Discussion

By heating the W filament it is promoted a spreading of spheres on the Pyrex glass. The spheres are composed by poorly crystallized $W_{25}O_{73}$, revealing that the tungsten is not well crystallized during the HFCVD deposition, this was mainly due to fact that during deposition, it is expected a temperature gradient in the neighboring of

Table 2
Sorption structural parameters of the same PTO sample under different thermal treatments.

Outgassing temperature (°C)	A_{SB} ($m^2\ g^{-1}$)	V_Σ ($cm^3\ g^{-1}$)	NLDFT adsorption mode pore size (nm)	NLDFT desorption mode pore size (nm)
120	38.67	0.121	10, 22, 30, 63	12, 22, 30, 63
200	37.91	0.098	12, 22, 50, 63	12, 22, 63
300	34.31	0.110	8, 16, 80, 63	12, 18, 63
400	34.51	0.109	18, 30, 63	12, 16, 30, 63

Specific BET surface area (A_{SB}); V_Σ is the total pore volume determined close to saturation ($p/p^0 \sim 0.95$) and calculated as volume of liquid.

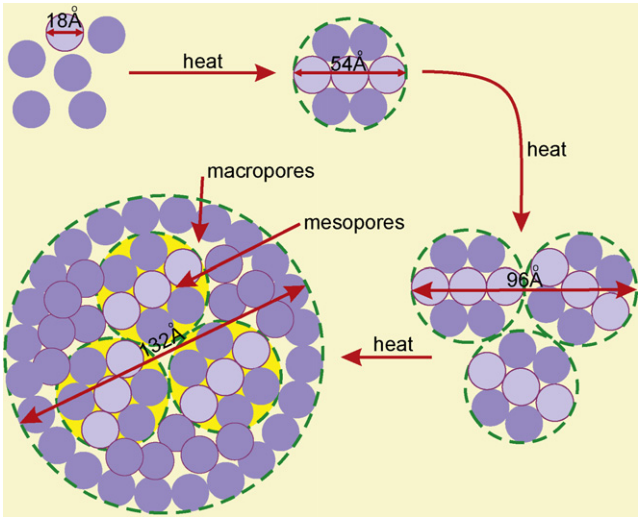

Fig. 7. A simple model of the agglomeration process to form a 3D porous network due to heating of the PTO film.

filament. Actually, a reaction that was carried out during the heating of the filament in the presence of some residual water contained in the system is as follows:

$$W_{(s)} + (3-X)H_2O_{(g)} \rightarrow WO_{(3-X)(g)} + (3-X)H_{2(g)}$$

The spheres fall randomly as a rain on the glass surface. Some spheres fall on other similar spheres, forming bigger aggregates. With variation in temperature, the dynamic in this primary aggregates enhances the sphere–sphere interactions and then they distribute in the space and connect in a form that they form other spheres, bigger as detected within the limits of the SAXS technique. It was not possible to match the SAXS results with SEM images. To obtain directly high-resolution images, at sub-micron scale, which required the use of specialized facilities (laser scanning focal microscopy). Actually, on the basis of the distribution of sizes of spheres, determined by SAXS, it can be proposed a simple model, which is shown in Fig. 7. The maximums of sphere sizes are shown in Fig. 5 that are very close to those can be obtained by joining a finite number of spheres; however, the connectivity of spheres and the change of crystalline phases cause changes in the fractal dimension and then the value of big spheres is not exactly a multiple of the small ones. An increase of fractal dimension parameter with temperature confirms that spheres are more and more interconnected. In other words, the geometrical figure is maintained but bigger objects are formed which are not perfect spheres but they present pores and defects that are highly desirable in materials with potential properties to be used as catalysts. The aggregation of small spheres generated free spaces between them. Fig. 7 represents a simple model that suggests the route how these free spaces are generated. In this sense the nitrogen adsorption–desorption isotherms are more informative as they are significantly altered with the evolution of the porous media. As the temperature of thermal treatment increases the surface of the sample is completely, or nearly, uniform in an energetic sense, this uniformity leads to the development of a step in the PTO heated at 300 °C which is a step-shaped isotherm type VI [38].

In general the porous network of the PTO sample is composed of quasi-independent pore domains because both the adsorption and desorption curves (Fig. 6a–d) do not show abrupt change in slope, so pore hysteresis rather than network hysteresis is prevailed [14].

The nanospheres of PTO have a tendency to stick together to form aggregates; this aggregation process is accelerated with temperature. Thus, the area is reduced by an amount equal to the area lost by formation of nanosphere-to-nanosphere joints, which was evidenced also by the increasing of the fractal dimension. Nevertheless, this is not a negative item of these materials because, a porous network with defects was created. The pore structure of this class of aggregates contains two kinds of holes; i.e. cavities between nanospheres (mesoporous) and between the clusters (macroporous), then the PSD occur over a wide range of pores sizes.

With increasing of temperature, not only the texture is altered but also the structure, as confirmed by X-ray thermodiffraction. This result was expected due to enhancing of desorption of water molecules by heating permits that these molecules to act as oxidizing agents of partially oxidized tungsten. The reaction of oxidation is endothermic and then favoured with the energy provided, thus at temperatures as high as 600–800 °C the oxidation is completed.

5. Conclusion

A porous tungsten oxide film containing spheres was grown on glass substrates throughout the HFCVD technique. Packed particles are distributed randomly on the substrate resulting in a 3D porous network with open spaces between the particles and clusters-like morphology. As the temperature increase, the BET surface of the film decreases from 38.67 to 34.5 $m^2\,g^{-1}$ because the spheres have a tendency to stick together to form bigger clusters. The heating of sample favored thermodynamically, the oxidation of tungsten and oxygen-deficient oxides leading an array of bigger packing spheres of crystalline WO_3. Furthermore, this array of self-organized porous tungsten oxide could be effectively applied in several fields such as catalysis and optical.

Acknowledgments

This research was supported by the Secretaría de Investigación y Posgrado (SIP-IPN), the Vicerrectoria de Investigación y Estudios Posgrado (VIEP-BUAP) and the Red de Fisicoquímica de Sistemas Complejos Nanoestructurados (PROMEP-SEP). Thanks to Nicolás Morales and A. Tejeda for his technical help.

References

[1] G. Gu, B. Zheng, W.Q. Han, S. Roth, J. Liu, Nano Lett. 2 (2002) 849.
[2] R.G. Palgrave, I.P. Parkin, New J. Chem. 30 (2006) 505.
[3] S. Vaddiraju, H. Chandrasekaran, M.K. Sunkara, J. Am. Chem. Soc. 125 (2003) 10792.
[4] Y. Baek, K. Yong, J. Phys. Chem. C 111 (2007) 1213.
[5] J. Polleux, M. Antonietti, M. Niederberger, J. Mater. Chem. 16 (2006) 3969.
[6] F. Huguenin, E.R. Gonzalez, O.N. Oliveira, J. Phys. Chem. B 26 (2005) 12837.
[7] A. Ponzoni, E. Comini, G. Sberveglieri, J. Zhou, S.Z. Deng, N.S. Xu, Y. Ding, Z.L. Wang, Appl. Phys. Lett. 88 (2006) 203101.
[8] F. Chávez, C. Felipe, E. Lima, E. Haro-Poniatowski, C. Ángeles-Chávez, O. Goiz, R. Peña-Sierra, M.A. Camacho-López, Mater. Lett. 62 (2008) 4191.
[9] Y.H. Li, Y.M. Zhao, R.Z. Ma, Y.Q. Zhu, N. Fisher, Y.Z. Jin, X.P. Zhang, J. Phys. Chem. B 110 (2006) 18191.
[10] P.M. Parthangal, R.E. Cavicchi, C.B. Montgomery, S. Turner, M.R. Zachariah, J. Mater. Res. 20 (2005) 2889.
[11] J.H. Park, O.O. Park, S. Kim, Appl. Phys. Lett. 89 (2006) 163106.
[12] D. Caiteanu, E. György, S. Grigorescu, I.N. Mihailescu, G. Prodan, V. Ciupina, Appl. Surf. Sci. 252 (2006) 4582.
[13] L.F. Reyes, A. Hoel, S. Saukko, P. Heszler, V. Lantto, C.G. Granqvist, Sens. Actuators B 117 (2006) 128.
[14] C. Felipe, F. Rojas, I. Kornhauser, M. Thommes, G. Zgrablich, Ads. Sci. Tech. 24 (2006) 623.
[15] P. Yang, D. Zhao, D.I. Margolese, B.F. Chmelka, G.D. Stucky, Nature 396 (1998) 152.
[16] G.M. Dhar, B.N. Srinivas, M.S. Rana, M. Kumar, S.K. Maity, Catal. Today 86 (2003) 45.
[17] A. Olivas, E.C. Samano, S. Fuentes, Appl. Catal. A: Gen. 220 (2001) 279.
[18] A. Montesinos-Castellanos, E. Lima, J.A. De los Reyes, V. Lara, J. Phys. Chem. C 111 (2007) 13898.
[19] M.G. Falco, S.A. Canavese, N.S. Fígoli, Catal. Today 107–108 (2005) 778.
[20] B. Gao, Y. Ma, Y. Cao, W. Yang, J. Yao, J. Phys. Chem. B 110 (2006) 14391.
[21] A.A. Ashkarran, A. Iraji zad, M.M. Ahadian, S.A. Mahdavi Ardakani, Nanotechnology 19 (2008) 195709.

[22] F. Di Fonzo, A. Bailini, V. Russo, A. Baserga, D. Cattaneo, M.G. Beghi, P.M. Ossi, C.S. Casari, A. Li Bassi, C.E. Bottani, Catal. Today 116 (2006) 69.
[23] S. Berger, H. Tsuchiya, A. Ghicov, P. Schmuki, Appl. Phys. Lett. 88 (2006) 203119.
[24] S. Pal, C. Jacob, J. Mater. Sci. 41 (2006) 5429.
[25] S. Pal, C. Jacob, Appl. Surf. Sci. 253 (2007) 3317.
[26] M. Deepa, A.K. Srivastava, K.N. Sood, S.A. Agnihotry, Nanotechnology 17 (2006) 2625.
[27] J. Lou, B.J. Ye, H.M. Weng, H.J. Du, Z.B. Wang, X.P. Wang, J. Phys. D: Appl. Phys. 41 (2008) 155410.
[28] S.F. Durrant, B.C. Trasferetti, J. Scarmínio, C.U. Davanzo, F.P.M. Rouxinol, R.V. Gelamo, M.A. Bica de Moraes, Thin Solid Films 516 (2008) 789.
[29] O. Glatter, J. Appl. Cryst. 14 (1981) 101.
[30] O. Glatter, B. Hainisch, J. Appl. Cryst. 17 (1984) 435.
[31] O. Glatter, J. Appl. Cryst. 21 (1988) 886.
[32] O. Glatter, Prog. Colloid Polym. Sci. 84 (1991) 46.
[33] O. Glatter, K. Gruber, J. Appl. Cryst. 1 (26) (1993) 512.
[34] M. Kataoka, J.M. Flanagan, F. Tokunaga, D.M. Engelman, in: B. Chanse, J. Deisenhofer, S. Ebashi, D.T. Goodhead, H.E. Huxley (Eds.), Synchrotron Radiation in the Biosciences, Clarendon Press, Oxford, UK, 1994.
[35] I.A. Ibarra, S. Loera, H. Laguna, E. Lima, V. Lara, Chem. Mater. 17 (2005) 5763.
[36] A. Harrison, Fractals in Chemistry, Oxford University Press, New York, 1995.
[37] S.J. Gregg, K.S.W. Sing, Adsorption, Surface Area and Porosity, Academic Press, London, 1982.
[38] K.S.W. Sing, D.H. Everett, R.A.W. Haul, L. Moscou, R.A. Pierotti, J. Rouquerol, T. Siemiewska, Pure Appl. Chem. 57 (1985) 603.
[39] P.I. Ravikovitch, A.V. Neimark, J. Phys. Chem. B 105 (2001) 6817.